Available online at www.eccomasproceedia.org
Eccomas Proceedia COMPDYN (2017) 3062-3073

ECCOMAS
Proceedia

COMPDYN 2017
6th ECCOMAS Thematic Conference on
Computational Methods in Structural Dynamics and Earthquake Engineering
M. Papadrakakis, M. Fragiadakis (eds.)
Rhodes Island, Greece, 15–17 June 2017

THE EFFECT OF HIGH IMPACT WHEELS ON RAIL FAILURE

Harry Tournay[1], **Semih Kalay**[2]

[1] Senior Scientist, Transportation Technology Center, Inc.
55500 DOT Road, PO Box 11130, Pueblo, CO, USA 81001
e-mail: harry_tournay@aar.com

[2] Sr. Vice President Technology, Transportation Technology Center, Inc.
55500 DOT Road, PO Box 11130, Pueblo, CO, USA 81001
e-mail: semih_kalay@aar.com

Keywords: Rail, Fracture, Failure, High Impact Wheels, Wheel Loads, Thermal Stress, Residual Stress, Reverse Bending, Indirect Loading, Head Defects, Transverse Defects, Base Defects, Fracture Mechanics, Wheel Impact Load Detectors, Track Modulus, Track Damping, Ties, Wheels.

Abstract. *Rail is subject to repeated load cycles and wear. These load cycles can induce fatigue and rail failure. As rail failure is less predictable, wear is the desirable failure mode and factors influencing rail failure are carefully managed by railroads. In North America, static wheel loads are limited to a nominal maximum of 159 KN; however, wheel treads can develop rolling contact fatigue resulting in so-called high impact wheels (HIW) that, before removal, can introduce high impact loads on the rail in excess of 700 KN.*

Transportation Technology Center Inc. (TTCI) was tasked by the Association of American Railroads (AAR) to determine the effect of HIW on rail failure and ascertain whether more stringent removal criteria should be applied.

TTCI conducted extended high frequency strain measurements at a WILD site and related the measured strains to the dynamic impact loads by the WILD site. These measurements supported analytical models developed to simulate defect growth and rail failure.

Results of the analysis suggest that HIW have a minimal effect on rail failure because of:

- *High attenuation of the bending wave under impact due to the high damping in the track.*
- *The low probability of repeated HIW cycles on specific elements within the rail.*

This paper describes the measurement and analysis process as well as the development of the models and the interpretation of resulting data and conclusions drawn.

Peer-review under responsibility of the organizing committee of COMPDYN 2017.
doi: 10.7712/120117.5626.16725

1 INTRODUCTION

Rail is subject to fatigue and wear. Fatigue failure is unpredictable so wear is the desired rail replacement mode. Factors influencing rail life are carefully managed by North American railroads including the loads to which the rail is subjected. Nominal static axle loads are limited to 32t (159kN wheel load); however high impact wheels (HIW) can occur, resulting generally from rolling contact fatigue of the wheel tread. HIW are difficult to predict and are detected at wheel load impact detectors (WILD) and generally removed from service at a HIW load 400kN. Outliers, may, however, remain in service for a limited time.

The possible role of HIW in rail fracture together with the 400kN limit and potential restrictions on outliers is being questioned by the railroads. This paper reports on an investigation into the effect of HIW on fracture from transverse defects (TD) and, by implication, fracture from defects in the running surface of the rail. Investigations continue into the effect of HIW on fracture from under-head and base defects.

2 RAIL STRESSES

Rail is subject to three main stress regimes that can be of similar magnitude:

- Vertical and lateral stresses associated with wheel loads and the bending of the rail as a continuous beam on resilient supports.
- Thermal stresses. Continuously welded rail is laid at a so-called neutral temperature associated with climatic conditions and a compromise made between compressive stresses under high ambient temperatures that could result in track buckling and low ambient temperatures resulting in tensile stresses and the potential for rail breaks.
- Residual compressive and tensile stresses due to rail straightening after heat treatment during manufacture and residual compressive stresses due to wheel / rail rolling contact.

2.1 Stresses due to wheel loads

The rail forms a continuous beam on resilient foundations. Wheel loads result in bending directly under the wheel and so-called reverse bending both in advance of, and behind the wheel (Figure 1).

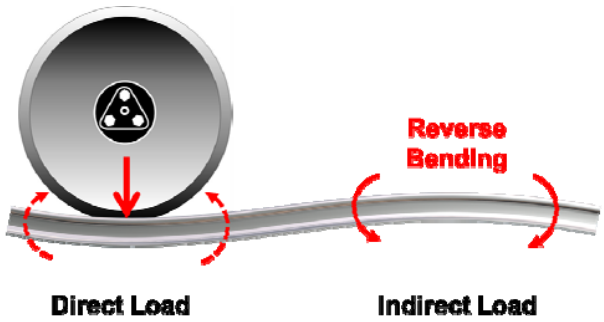

Figure 1. Direct loading and indirect loading (reverse bending) of the rail resulting from a single wheel load on a rail supported by an elastic foundation.

The rail is subjected, typically, to 5 nominal reverse bending cycles as each coupled pairs of wheels in typical railway bogies pass a point on the rail. Figure 2 shows a typical resulting bending moments in the rail due to nominal wheel loads.

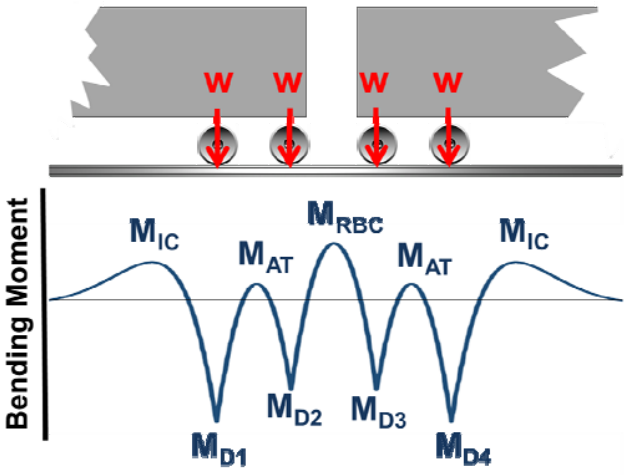

Figure 2. Typical bending moment distribution produced by four wheels across the ends of two coupled wagons.

Moments due to direct loading are a function of the wheel load; that is:

$$M_{DN} \approx f(W_{DN}) \quad \text{..... (1)}$$

Moments due to reverse bending are:

- M_{RC} (reverse bending between bogies in a wagon)
- M_{RT}, (reverse bending between wheels in a bogie)
- M_{RV} (reverse bending between coupled wagons)

These moments are a function of both the magnitude and proximity of adjacent wheel loads. The maximum reverse bending moment resulting in tension in the rail head (the driver of transverse defects in the head) occurs typically between cars (Figure 2).

As each coupled truck pair passes a point in the rail, alternating stress cycles are generated, ranging from tension through compression. These cycles are associated with rail fatigue (and crack growth if there is a defect).

The objective of this investigation was to determine the role of intermittent HIW on rail stresses and whether, possibly in combination with thermal and residual stresses (2.2 and 2.3 below), HIW can lead to premature rail fracture.

2.2 Thermal Stresses

Rail is laid at a neutral temperature (RNT) determined by the climate of the region of the track. Temperature differences between the RNT and ambient generate rail thermal stresses, σ_t, are assumed to be uniformly distributed through the rail section and approximately equal to:

$$\sigma_t = E\alpha\,\Delta T \quad \text{..... (2)}$$

where:

ΔT = temperature difference: ambient and RNT.

E = Young's Modulus for steel.

α = Coefficient of thermal expansion for steel.

2.3 Residual Stresses

Residual stresses can result from both initial manufacture (roller straightening) and in-service cold rolling due to repeated wheel loads. Roller straightening induces tension in the rail head and base (Figure 3) [1]. Repeated wheel loads can induce residual compression in the running surface of the rail (Figure 4) [4]. This leaves, generally, a region of tensile residual stress in the centre of the rail head.

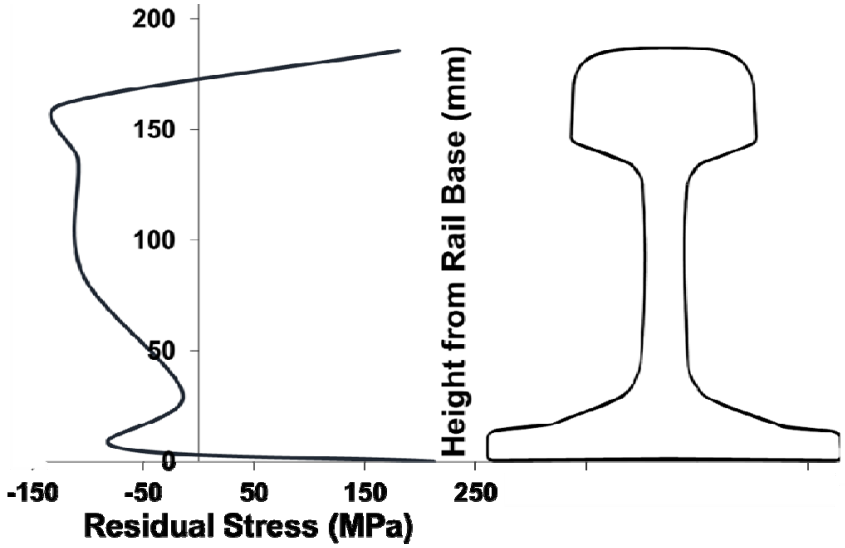

Figure 3. Measured residual stresses in the rail section due to roller straightening.

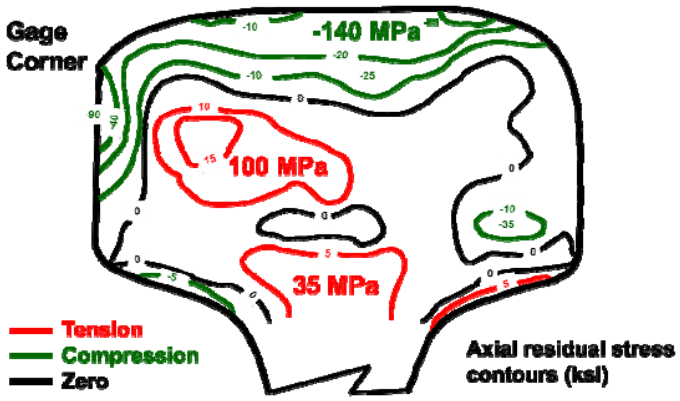

Figure 4. Axial residual stresses in the rail head due to roller straightening & service wheel loads.

3 STRESSES AT A POINT IN THE RAIL

3.1 Fatigue

In rail assumed to have no measurable macro-defects, rail fatigue is determined by the magnitude of the stress amplitude, S_a, where:

$$S_a = (S_{max} - S_{min}) / 2 \quad \text{.....} \quad (3)$$

Figure 5 defines S_{max} and S_{min}: and implies that rail fatigue is driven mainly by alternating stresses resulting from wheel loads and not by static thermal & residual stresses.

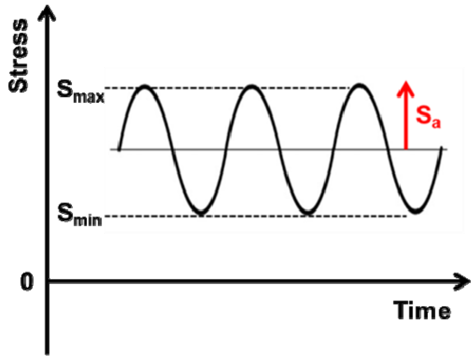

Figure 5. Variable stress amplitude, S_a due to wheel loads is the driver of fatigue in a rail with no measurable defects.

3.2 Crack growth and fracture from a defect

When a defect is present in a rail, crack growth and ultimate fracture is driven by the stress at the crack tip and close vicinity. These tresses are driven by the combination of bending as well as thermal and residual stresses, Figure 6.

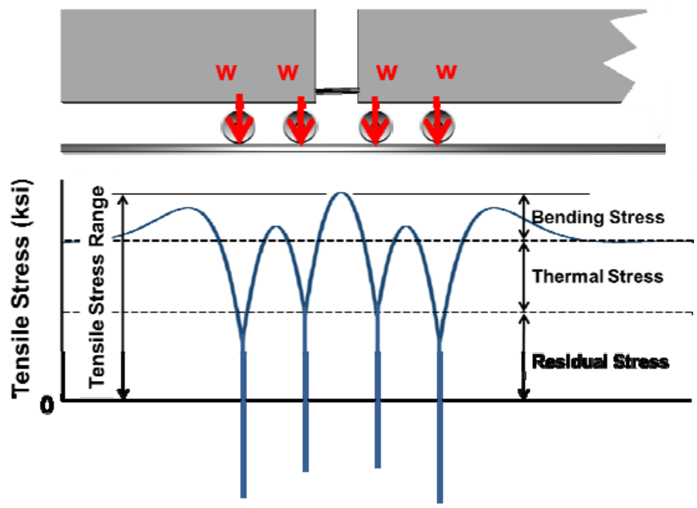

Figure 6. A combination of stresses due to wheel loads, and thermal and residual stresses is the driver of crack growth and fracture in a rail with a pre-existing defect

Fracture may occur when the stress intensity fracture (K_1) exceeds the critical stress intensity factor, or fracture toughness, K_{IC}. This is expressed as:

$$[\sigma_t + \sigma_r + \sigma_w] (\pi a)^{½} g - K_{IC} < 0 \quad (4)$$

Equation 4 is quoted in different forms in fracture mechanics literature (Kuna 2010) where:

K_{IC} = Critical stress intensity factor, or fracture toughness of the rail material
σ_t = Thermal stress
σ_r = Residual stress
σ_w = Stress from wheel loads
a = Defect / crack size
g = Factor describing the crack geometry

The basis for equation 4 may also be used to express crack growth rate.

Equation 4 suggests that crack growth and fracture occurs at a location where $[\sigma_t + \sigma_r + \sigma_w]$ are maximized in combination with g and defect size, a.

4 SERVICE TESTS

Wheel loads and associated rail stresses were measured at a typical WILD site on 97 km/h (60 mph) track with 67.5 kg/m (136RD) rail on concrete sleepers and Pandrol fasteners. A WILD site comprises three instrumented crib groups on each rail. Strain gages were placed between two instrumented crib groups as Figure 7 indicates. Gages were placed to measure longitudinal strains. Strains at the under-head locations (gage and field side) were monitored individually (Figure 8). Strain gages on the rail base were connected on a common circuit, producing an averaged strain signal.

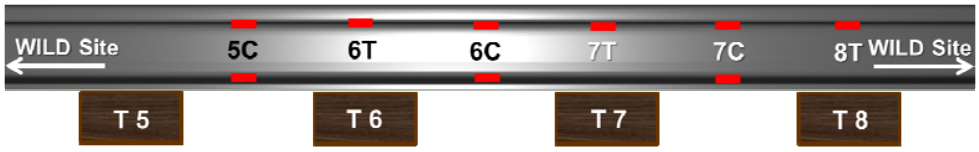

Figure 7. Gages placed between two instrumented groups

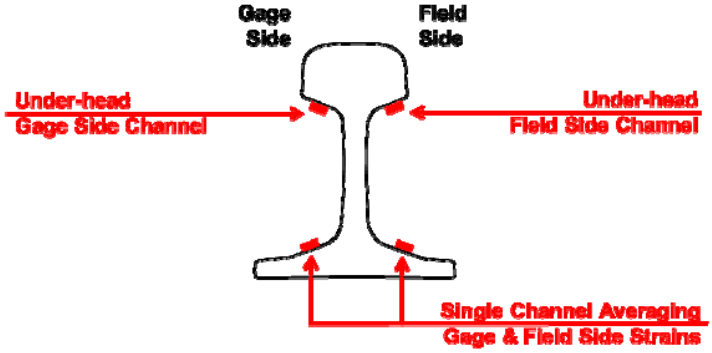

Figure 8. Strain gage locations over a crib

Strains were measured at an acquisition rate of 10K Hz and filtered at a frequency of 3 KHz. The WILD site vendor then provided dynamic wheel load data and the crib locations associated with each wheel load. TTCI then identified the loads (static and dynamic) bearing on the TTCI instrumented cribs. Wheel loads, W, and corresponding direct and indirect loading strains were then merged to produce strain profiles per wheel load.

Tests were conducted in:

– *Summer* when the track modulus was relatively soft (7–14 MPa). More than 17,000 wheelset passes were monitored; however, a limited number of HIW were measured as HIW are more prevalent in winter.
– *Winter* when the track modulus was at least 3 times harder (estimated from very approximate deflection measurements to be > 40 MPa). The ballast and formation was observed to be frozen with minimal rail vertical deflection. More than 96,000 wheelset passes were monitored in an attempt to capture as many and an increased number of HIW were measured.

Figure 9 shows the measured wheel load spectra.

Measured wheel load distributions were bi-modal, reflecting empty and loaded wagons, typical for North American WILD sites. The data also reflected the increased incidence of HIW in winter (typically > 200kN).

Measured stresses never exceeded approximately 90 MPa. Figure 10 shows an example of the summer and winter stress spectrum measured on the top of the base of the rail.

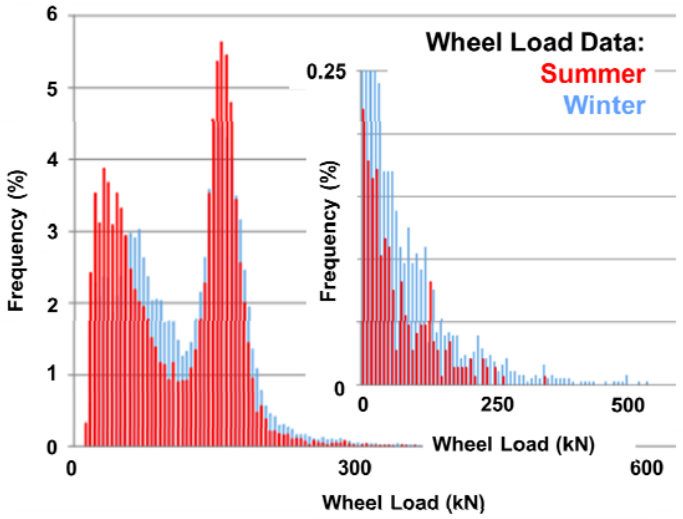

Figure 9. Summer and winter wheel load spectra at WILD site

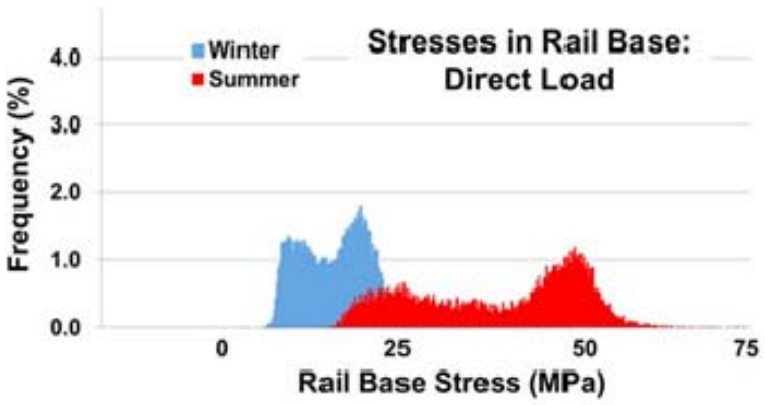

Figure 10. Example of rail stresses under the load spectrum indicated in Figure 9

It was concluded that the frequency and magnitude of the stresses due to HIW will not reduce the fatigue life of the rail beyond that attributed to nominal wheel loads.

Further observations from the service data suggest that the rail stresses under indirect load (reverse bending) reach a plateau beyond a wheel load of approximately 180kN (Figure 11).

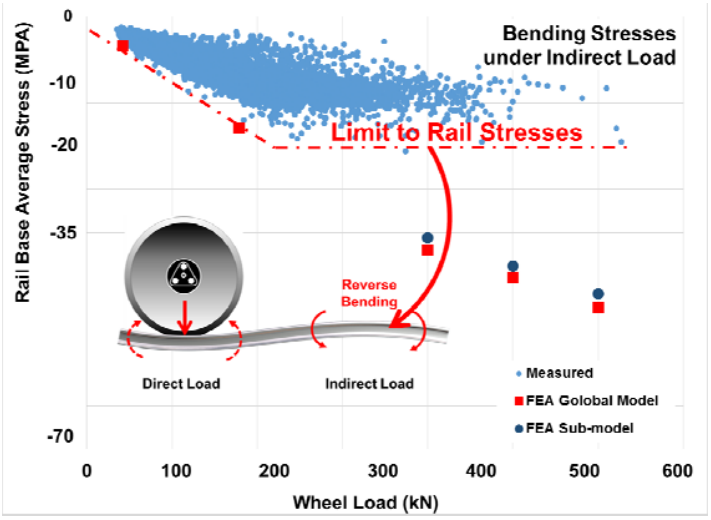

Figure 11. Measured stresses under indirect loading reach a maximum at a load of approximately 180kN

Stresses do not increase as predicted by the theory of a continuous beam on elastic foundation or the assumed bi-linear stiffness and hydraulic damping model in the track model used in the finite element analysis (FEA) of rail stresses (see data points associated with FEA global and sub-model in Figure 11).

Examination of the stress-time histories suggests that the root cause for this "plateauing effect" is the attenuation of the bending stresses.

Figure 12 shows the rail stresses under the impacting wheel at the time of impact. The influence if the impacting wheel is evident in relation to the stress peaks attributable to the "nominal" wheel loads.

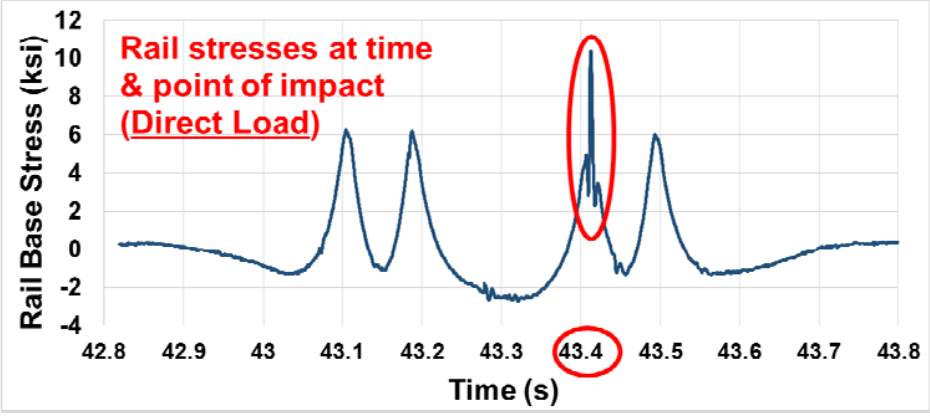

Figure 12. Rail stresses at point and time of impact of a HIW

Figure 13 shows the rail stresses at a point approximately 0.6 m away from the point of impact.

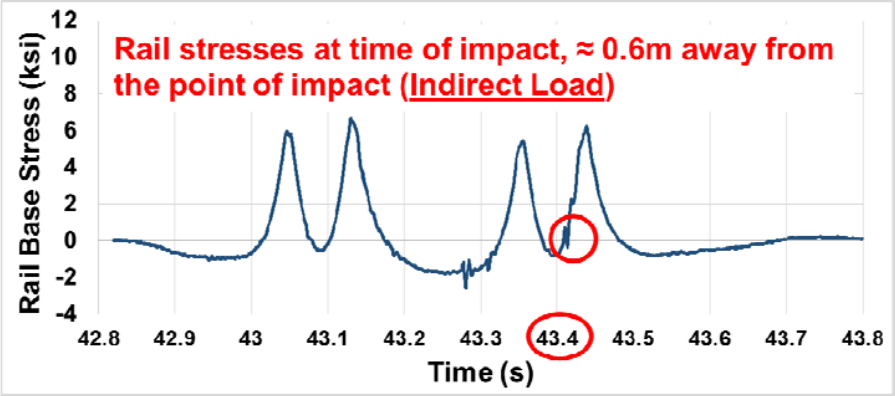

Figure 13. Rail stresses at time of impact shown in Figure 10, but approximately 0.6 m away from the point of impact

Two effects are apparent from Figures 10 and 11:

- The bending in the rail due to the impact load is almost completely attenuated.
- The little bending that is evident in the rail does not coincide with a peak bending due to a nominal wheel load. This is due to the difference in speed of the propagated bending wave due to the impact load and the speed of the wheels of the train producing the nominal wheel loads.

The significant conclusion to be drawn from these measurements is that the rail at the test site "sees" a HIW load in reverse bending very much as it "sees" a nominal wheel load. Consequently, transverse defects in the rail head that are subject to tensile stresses under reverse bending should not experience higher growth rates or fracture than that due to nominal wheel loads.

This finding may be generally true for rail on concrete ties in North America. However, it needs to be verified for the many different track types in North America and suggests the need for the development of a more complex track model to simulate HIW loads. This model probably needs to simulate at least sub-tie and rail pad stiffness and damping.

5 FRACTURE MECHANICS ANALYSES

Notwithstanding the findings on the limitations of the track model used, two fracture mechanics analyses were conducted using:

- A rail-specific fracture mechanics program called *RailGrow*. (Reference Section 5, Acknowledgements).
- A Finite Element Analysis of a penny-shaped crack simulating a transverse defect in the rail head.

5.1 RailGrow Analysis

RailGrow is a fracture mechanics program that can simulate the growth rate of, amongst others, a transverse defect in a rail subject to bending stresses from wheel service load spectra, thermal stress spectra and assumed residual stress distributions in the rail head. Track modulus, rail sectional properties, and rail material are input together with fracture mechanics properties, defect size, shape, and position. Crack growth is predicted to failure under wheel and thermal overload conditions. The rail is assumed to be a continuous beam on elastic foundation, which was found to be over-predictive of the effect of HIW loads as discussed in Section 4.

Using *RailGrow*, a transverse defect was "grown" in the rail head under a specific load regime. At every 0.0254 mm of crack growth, the rail was subjected to a single HIW and a thermal overload. Critical crack sizes under the final fracture load applied in the laboratory were compared with a number of published laboratory test results, Igwemezie et al. 1993 (example: Figure 14).

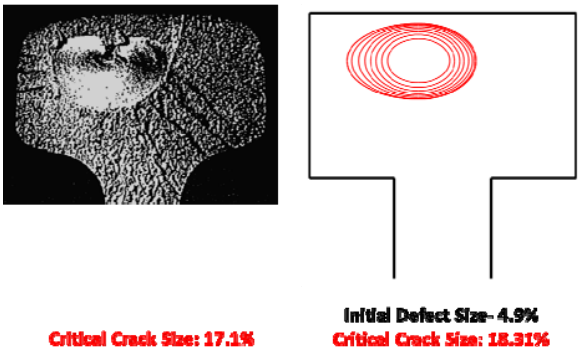

Figure 14. *RailGrow* simulated crack growth to failure "calibrated" against laboratory a test of fracture of a rail with pre-existing transverse defect under thermal and impact loads

The *RailGrow* model was then used to grow transverse defect cracks to critical sizes under different thermal and HIW overload conditions. Figure 15 shows the results of this analysis. The relationship between critical crack size of a transverse defect and the level of prevailing HIW is "flat" and is more a function of the temperature of the rail below the neutral laying temperature.

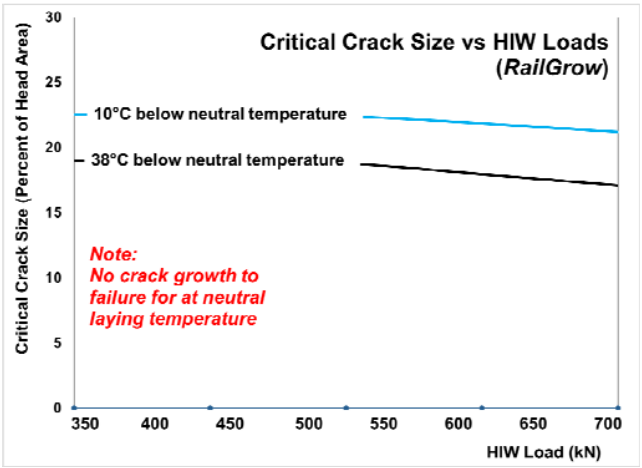

Figure 15. Critical crack size versus overload conditions predicted using RailGrow

5.2 Finite Element Analysis

Two basic finite element models of the rail were built:

– A so-called "global model" representing an approximately 25 m long section of rail subject to four point loads representing the wheel loading that Figure 2 depicts; one wheel simulating the HIW load, the other three point loads simulating nominal wheel loads.

– A shorter sub-model directly under the impacting wheel and including a section of rail under reverse bending. This model used boundary conditions developed from the global model with a segment of wheel being used to apply the HIW load.

The finite element model of the rail was supported at a typical tie spacing using a model that Figure 16 shows:

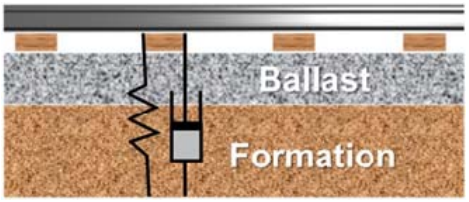

Figure 16. Track Model

The stiffness under each tie was modelled using a bi-linear spring / damper system in compression with different properties under uplift conditions.

A penny-shaped crack simulating a transverse defect was introduced in the sub-model (Figure 17) and crack tip stresses and KI values (crack tip energy in the axial tension mode) were determined for increasing HIW loads and rail; temperatures were below the rail neutral temperature.

As with the *RailGrow* analysis, the propensity for failure is "flat" with HIW load and more a function of the temperature below the rail neutral temperature (Figure 18).

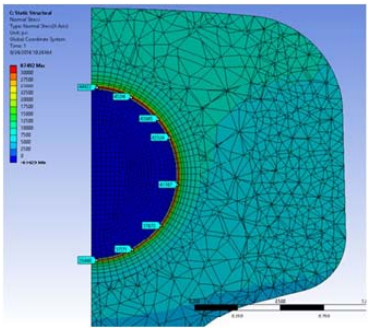

Figure 17. Example of mesh and output from the analysis of a penny-shaped crack in the rail head

Consequently, fracture mechanics analyses show no relationship between HIW and the fracture of rail from typical transverse defects in the rail head; this, even given that the fracture mechanics models over- predict the stresses in the rail head under reverse bending.

CONCLUSIONS

TTCI has conducted extensive tests and analyses to determine the effect of HIW loads on rail failure from transverse defects in the head of the rail.

Measured stress maxima associated with HIW loads in revenue service were found to be too low and infrequent to reduce rail fatigue life and that any fracture must be initiated from pre-existing defects, for example, transverse defects.

Fracture from transverse defects in the rail head can only be activated by the reverse bending mode in the rail. This mode occurs both in advance and behind the wheel.

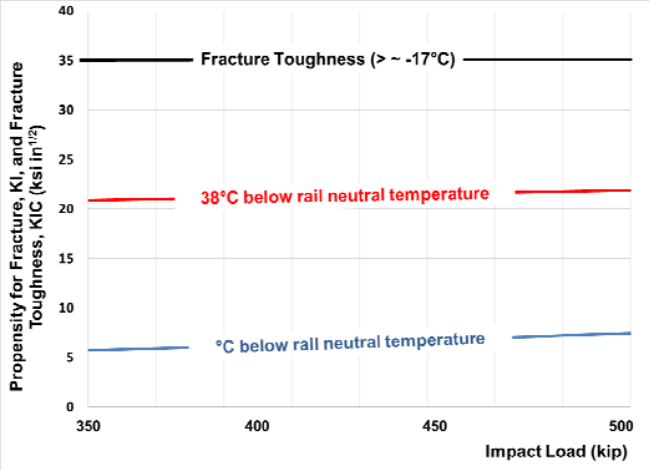

Figure 18. Plot of the energy at the tip of a penny-shaped crack in the rail head versus HIW load and temperature below the rail neutral laying temperature

Tests show that on track constructed of concrete sleepers on rail pads and secured with rail clips, the reverse bending mode is attenuated under dynamic wheel loads higher than 20kN. In other words, the rail "sees" a HIW load as any other service loaded wheel load of up to 20kN.

Two fracture mechanics models or approaches have been developed. These models have been shown not to simulate the attenuation measured in test and, consequently, will over-predict the effect of HIW loads. Both models show no effect of HIW on rail failure from transverse defects in the rail head.

Consequently, TTCI has found no evidence of an effect of HIW on rail failure from HIW.

ACKNOWLEDGMENTS

The authors thank:

- Canadian National Railway and staff for facilitating the tests at Calrin WILD site.
- Retired Prof. Darrell Socie of the University of Illinois Urbana Champaign who developed the rail fracture mechanics program, *RailGrow*, under contract to TTCI and based on work done by the Volpe, The National Transportation Systems Center and funded by the office of the Federal Railroad Administration.
- Many TTCI staff in support of this project.

REFERENCES

1. Gutscher, D. (2010, March). Railhead repair weld residual stress investigation. *Technology Digest* TD-10-007. Pueblo: AAR/TTCI.
2. Igwemezi, J. O., Kennedy, S. L., Feng, X., & Cai, Z. (1993, June). Defective rail fracture under dynamic, thermal and residual stresses. In *Proceedings of 5th Intl. Heavy Haul Conf, Beijing, China* (pp. 6-13).
3. Kuna, M. 2013. *Finite elements in fracture mechanics*. Dordrecht: Springer.
4. Orringer, O., Morris, J. M., & Steele, R. K. (1984). Applied research on rail fatigue and fracture in the United States. *Theoretical and Applied Fracture Mechanics*, *1*(1), 23-49, North Holland.